Catalysis Science & Technology

Mechanistic insights into the conversion of polyalcohols over Brønsted acid sites

Journal:	*Catalysis Science & Technology*
Manuscript ID	CY-ART-04-2023-000524.R1
Article Type:	Paper
Date Submitted by the Author:	08-Jun-2023
Complete List of Authors:	Nguyen, Quy; University of Oklahoma, Chemical, Biological and Materials Engineering Chau, Han; The University of Oklahoma, Chemical, Biological and Materials Engineering Lobban, Lance; University of Oklahoma, Chemical, Biological and Materials Engineering Crossley, Steven; University of Oklahoma, Chemical, Biological and Materials Engineering Wang, Bin; University of Oklahoma, Chemical, Biological and Materials Engineering

ARTICLE

Mechanistic insights into the conversion of polyalcohols over Brønsted acid sites

Received 00th January 20xx,
Accepted 00th January 20xx

DOI: 10.1039/x0xx00000x

Quy P. Nguyen,[a] Han K. Chau,[a] Lance Lobban, [a] Steven Crossley,[a] Bin Wang*[a]

Multi-layered plastics (MLP) film provides excellent properties for food packaging; however, because of complicated chemistry of hydrophobic substrates and tightly laminated hydrophilic layers, it is challenging to recycle of the MLP films. Selective conversion of polar functional groups in hydrophilic layers with minimal destruction of the carbon backbone of constituted polymers is considered a promising approach to improve the recyclability of MLP films. In this work, we combine computational and experimental studies to investigate acid-catalyzed conversion of functional groups in polyalcohols, through which we report potential reaction pathways involved in the conversion of ethylenevinylalcohol (EVOH), a common copolymer used in MLP films as an oxygen barrier. Using 2,4-pentanediol as a model compound, we show that its conversion proceeds primarily through the dehydration of a hydroxyl group via either a stepwise or a concerted mechanism to form an unsaturated alcohol that can be further converted into a conjugated diene or a saturated ketone; this secondary reaction determines the product selectivity. The rate-determining intermediates and transition states are identified, and the activation barriers are calculated, in agreement with experimentally observed product selectivities. This work thus provides insights for the selective conversion of EVOH.

1. Introduction

A great challenge of recycling/upcycling single-use plastics is to convert multi-layered plastics (MLP) film that is used extensively in packaging industries to provide high-performance, multi-functional materials with reduced production/transportation cost[1, 2]. However, multi-layered plastics present a distinct challenge of recycling when contrasted with single resin polyolefins, which have been reported via catalytically functionalizing C-C bonds[3], alkane dehydrogenation and sequential olefin metathesis[4] or hydrogenolysis[5]. MLP recycling is much more challenging due to difference and complexity in chemistry of the hydrophobic substrates, like polyethylene (PE) and polypropylene (PP), and hydrophilic functional layers, such as polyethylenevinylalcohol (EVOH) and polyethylene terephthalate (PET), all of which are tightly laminated together into a very thin structure[6, 7]. This limits common options for MLP waste handling as incineration or landfill[8]. Recently, there has been extensive research to enhance the recyclability of MLP using solvents to separate and precipitate different layers[9-11], adding compatibilizers to improve the mechanical recycling[12], or catalytically pyrolyzing MLP into lower molecular weight compounds[13]. Nonetheless, each of these approaches require a significant amount of energy. Tie layers complicate solvent separation, which can be a time and energy intensive process. Compatibilizers are often expensive and limit post use application, and pyrolysis generates products that are typically greatly reduced in value when compared with the initial polymer. While continued advancement in each of these areas is essential, there are still much room for improvement to develop processes that can selectively convert the impurities while in parallel minimizing energy inputs and maximizing the overall amount of initial polymer that is ultimately recycled. One of the promising approaches is to selectively convert the functional groups in the minor component (such as EVOH) while minimizing cleavage of the hydrocarbon backbone. In accordance with that strategy, mechanistic insights into conversion of functional groups incorporated in the MLP film are thus very important.

As a commonly used oxygen barrier for MLP films, EVOH is a polar co-polymer[14], and its selective conversion to create a polymer that is compatible with the hydrophobic components in MLP films warrants investigation. On the polymeric systems, Thomas et al.[15] and Yang et al.[16] reported the conversion of hydroxyl groups during thermal degradation of polyvinylalcohol (PVA), which is a co-building block of EVOH. Some prior insight may be obtained from prior work with model compounds of EVOH structures containing density of OH groups that are analogous with some bio-derived model compounds. Sato et al.[17, 18] and Gnanamani et al.[19] reported conversion of hydroxyl groups in butanediols and pentanediols, respectively, over families of metal oxide-based catalysts. They observed that the partially dehydrated alcohol is the primary and major product with some minimal amount of ketone and cracking products. Kondo and co-workers employed metadynamics simulations to theoretically investigate the conversion of hydroxyl groups in hexane-2,5-diols, which is also a polyalcohol structurally

[a] School of Chemical, Biological and Materials Engineering, University of Oklahoma, Norman, OK 73019, USA
* Corresponding author: wang_cbme@ou.edu
Supplementary information available at DOI: 10.1039/x0xx00000x

analogous to repeated units of EVOH, using a hot acidic solution[20]. They reported 2,5-dimethyltetrahydrofuran as the primary product, further dehydration of which produces dienes. However, there have been limited studies to reveal the reaction mechanism, particularly the competition between dehydration and isomerization, in chemical transformation of EVOH or its model compounds in heterogeneous catalysis. Atomistic insights into the mechanism of conversion of neighboring hydroxyl functional groups remain elusive in the literature.

In this work, we report a combined computational and experimental study to investigate the conversion of functional groups in polyalcohols over Brønsted acid sites (BAS), through which we compare reaction pathways toward different products that are potentially involved in the EVOH conversion. Specifically, we probe the conversion of two neighboring hydroxyl groups of PVA (a co-building block of EVOH) over sulfonic-functionalized amorphous silica. 2,4-Pentanediol is used as the model compound based on the structural analogue in relative positions between -OH and -CH_2- groups with the repeating unit of PVA. We show that the dehydration at the first hydroxyl group can proceed through either a stepwise or a concerted mechanism to form an unsaturated alcohol intermediate that can be further converted into ketone and diene. The primary and secondary products are determined, and the rate-determining steps are identified. The calculations are supported by product selectivity in experiments. These results provide insights for converting EVOH as detailed in the discussion.

2. Methodology

2.1. Computational details

The Vienna Ab Initio Simulation Package (VASP)[21] was used to calculate all electronic energies based on density functional theory (DFT). Description of the electron-ion interactions was carried out using the projector-augmented wave (PAW)[22, 23] potential with a plane-wave energy cutoff of 400 eV. The generalized gradient approximation (GGA) with Perdew-Burke-Ernzerhof (PBE) exchange-correlation functional was used[24]. The van der Waals interaction was taken into account using the DFT-D3 semiempirical method[25]. Iteration of electronic self-consistency with 10^{-5}-10^{-7} eV and atomic force of -0.01 eV/Å were employed to optimize the structures. A 1×1×1 k-mesh centered at the G point was used to sample the Brillouin zone. To search for the transition states (TS), the Nudged Elastic Band (NEB)[26] method was performed to obtain the initial guesses, which were utilized for further optimizing using the DIMER[27, 28] method.

The vibrational frequencies for calculating the zero-point energy and vibrational entropy, and validating the TS structures were computed using the partial Hessian vibrational analysis (PHVA)[29]. The entropy change of adsorption and desorption was mostly attributed to a third of the translational entropy of the corresponding gas-phase molecules, which was computed according to the statistical thermodynamics[30], based on literature studies[31]. The entropic contribution in Gibbs free energy of intermediates and TS was calculated using the harmonic approximation (HA). Though HA could result in large errors in absolute values due to overestimated entropy

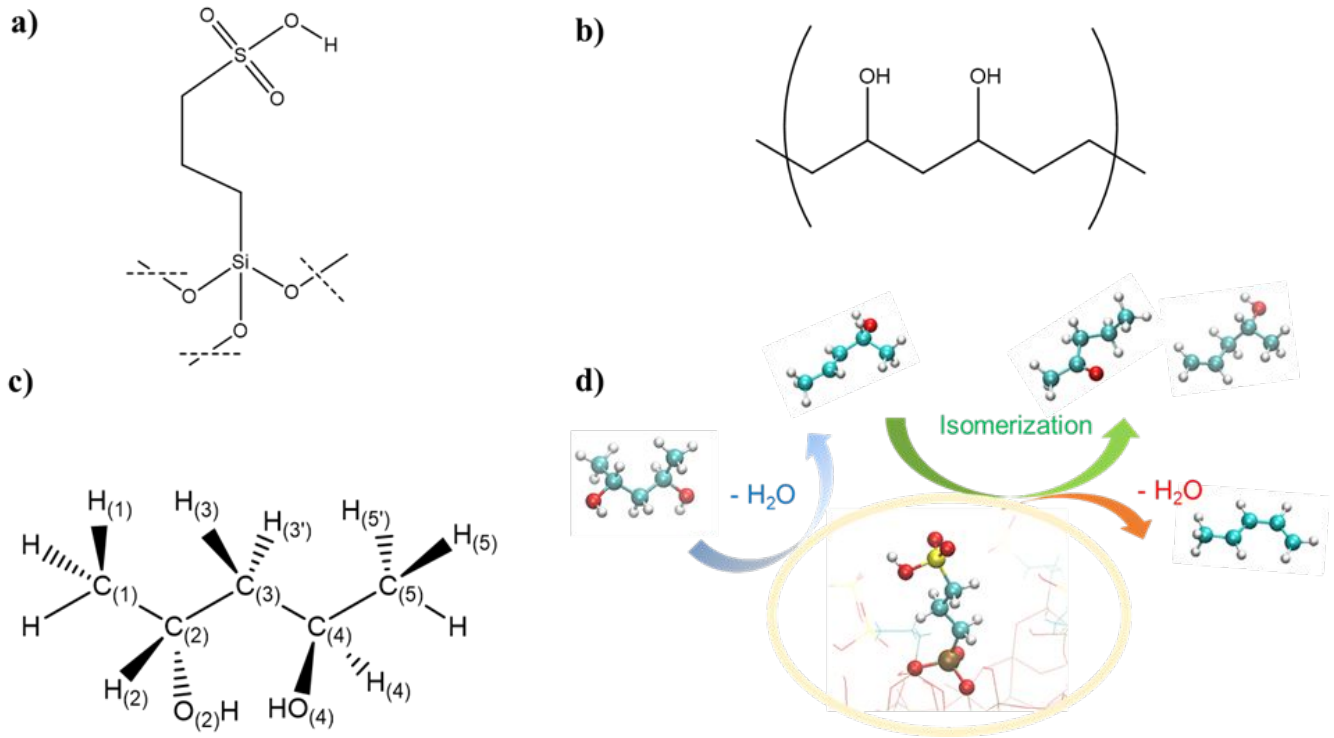

Figure 1. a) Catalyst 2D-model; **b)** 2D-Structure of a common type of EVOH in block arrangement of PVA and PE with 68% : 32% molar ratio; **c)** Index of atoms in 2,4-pentanediol – the diol model of PVA co-building block of EVOH. The same index is also applied for the products**; d)** Schematic reaction. The carbon, hydrogen, oxygen, silica, and sulfur atoms are colored, respectively, by cyan, white, red, brown, and yellow. From left to right on top of the BAS of a functionalized sulfonic group (in yellow ellipse): 2,4-Pentanediol proceeds the primary dehydration of a -OH group, resulting in 3-pentene-2-ol. This unsaturated alcohol is further activated and undergoes different secondary conversions including isomerization and dehydration, which lead to the formation of 2-pentanone, 4-pentene-2-ol, and pentadienes. Details in proposed reaction mechanism is shown in Figure 2.

change[31], it can still provide a reasonable reaction profile as the errors in the Gibbs free energy calculations of intermediate/TS could cancel out. There are also methods such as hindered translators/rotors models to improve the accuracy of entropy calculation[32-34]; however, their simulation time for a large system as in this study are significant. Therefore, to balance the accuracy and the efficiency of calculations, we utilized the HA method with imaginary and low-lying frequencies (< 50 cm^{-1}) normalized to 50 cm^{-1} as in the literature[35].

The enthalpy (H), entropy (S), and Gibbs free energy (G) were calculated at 500 K based on DFT-calculated energies and the statistical thermodynamics using DFT-calculated frequencies[30]. The energetic span model described by Kozuch et al.[36] was applied to determine the rate-determining intermediate (RDI) among all the surface species, the rate-determining transition state (RDTS), and the corresponding activation barrier.

2,4-pentanediol was used as the model compound to probe the conversion of two neighboring hydroxyl groups of a common EVOH (Figure 1b) that has 68% PVA and 32% PE of molar ratio. This model compound has similar relative positions of two neighboring OH groups with the repeating unit of PVA co-building blocks in EVOH.

A unit cell of amorphous silica containing 109 units of SiO_2 in the lattice with a = 21.4 Å, b = 21.4 Å, c = 50.0 Å (including a vacuum space of 30 Å in the z-direction)[37] was used as the model catalyst. We replaced a few silanol groups on top of the silica surface by six propylsulfonic groups as in our previous work[38]. The initial structure of this model catalyst was fully optimized. After that, a propylsulfonic group was introduced as the active site to probe reactions (Figure S1). In later calculations of activation barriers, only the active site and the adjacent SO_3H group relevant to the reaction (Figure S1) were allowed to move, and other atoms in the support were fixed. The 2D-model of the catalyst is shown in Figure 1a.

2.2. Experiment method

The details of catalyst preparation and characterization as well as external mass transfer limitation test are included in the Supporting Information. Based on the TGA-TPO method, the acid site density of the sulfonic acid-functionalized silica was obtained with 0.902 mmol/g sulfonic groups per gram catalyst, which is close to the acid density (0.772 mmol/g) used in the DFT calculations. The Vapor phase dehydration of 2,4-pentanediol was carried out in a quartz tube reactor (1/4" OD) at atmospheric pressure. The catalyst was mixed with acid-washed glass beads and packed between quartz wool layers in the quartz reactor. The quartz reactor was installed inside an oven whose temperature was controlled by a thermocouple inside the quartz reactor and beneath the catalyst bed. Before injecting reactants, the SiO_2-SO_3H catalyst was pretreated by heating to 250°C at the ramp rate of 10°C/min and held at 250°C for 1 hour to remove physisorbed water in the catalyst. The oven temperature was then set to reach the desired reaction temperature. Reactant (2,4-pentanediol) was injected into the reactor through a septum on a heated vaporization zone using KD Scientific syringe pumps. To prevent the condensation of reaction products on the downstream tubing, the outlet of the reactor was heated to 250°C. Samples were collected at different reaction time on stream (TOS) using a gas sample loop connected with a six-port valve and products were analyzed by a Hewlett Packard 6890 gas chromatograph equipped with a flame ionization detector and an INNOWAX column (30 m × 0.25 mm).

To decouple kinetic effects from catalyst deactivation over reaction time on stream in flow reactions, the conversion and product yields were extrapolated to zero-time on stream.

$$\text{Conversion (\%)} = \frac{\text{Molar flowrate of reactant (in)} - \text{Molar flowrate of reactant (out)}}{\text{Molar flowrate of reactant (in)}} \times 100\% \quad (1)$$

$$\text{Product yield (mol\%)} = \frac{\text{Product molar flow rate } \left(\frac{\text{mol}}{\text{s}}\right)}{\text{Reactant molar flow rate } \left(\frac{\text{mol}}{\text{s}}\right)} \times 100\% \quad (2)$$

$$\text{Product selectivity (\%)} = \frac{\text{Molar flowrate of target product}}{\text{Total molar flowrate of observed products}} \times 100\% \quad (3)$$

3. Results and discussion

The proposed reaction network is shown in Figure 2. It is noted that alongside the uni-molecular route, the dehydration of alcohols is also well-known to proceed through the bi-molecular pathway, in which another alcohol molecule would assist in protonating the adsorbate, eliminating the water molecule, and/or deprotonating the alkoxide intermediate[39-41]. In this study, however, since we focused on the chemistry and kinetic behavior of the selective conversions of a OH group with influence of another neighboring OH group in the same carbon chain, only the uni-molecular route is considered. Also, we excluded the intramolecular etherification resulting in a 4-member ring product that is very strained and unstable, which is thus not likely to be a competitive pathway. In addition, because there were no branched products observed in experiments discussed below, we think such reactions are not kinetically competitive under the reaction conditions of this study and their mechanistic studies are thus not included here.

For the dehydration of the first OH group, the adsorbed diol (I1) can undergo either the concerted route (E_2-like mechanism) or the stepwise pathway (E_1-like mechanism though the formation of alkoxide intermediate I2). This primary conversion leads to the formation of an unsaturated alcohol intermediate and a water byproduct that are physiosorbed on the surface (I3). The water byproduct that is physiosorbed on the adjacent SO_3H group (Figure S2) can then be removed from the surface, leading to the state of intermediate I4.

The unsaturated alcohol intermediate I4 could be activated at the same active site following two plausible ways: activation of the second hydroxyl group or activation of the C=C bond. When the OH activation takes place, due to the limited reaction coordinate, the adsorbed intermediate (I5) could only be dehydrated via an E_1-like mechanism to form the alkoxide (I6). This surface species is deprotonated at the terminal CH_3 group to form the conjugated diene (I7), which is finally desorbed. In case the primary product is activated at the C=C bond, the adsorbed state (I5') can proceed with either the C=C bond

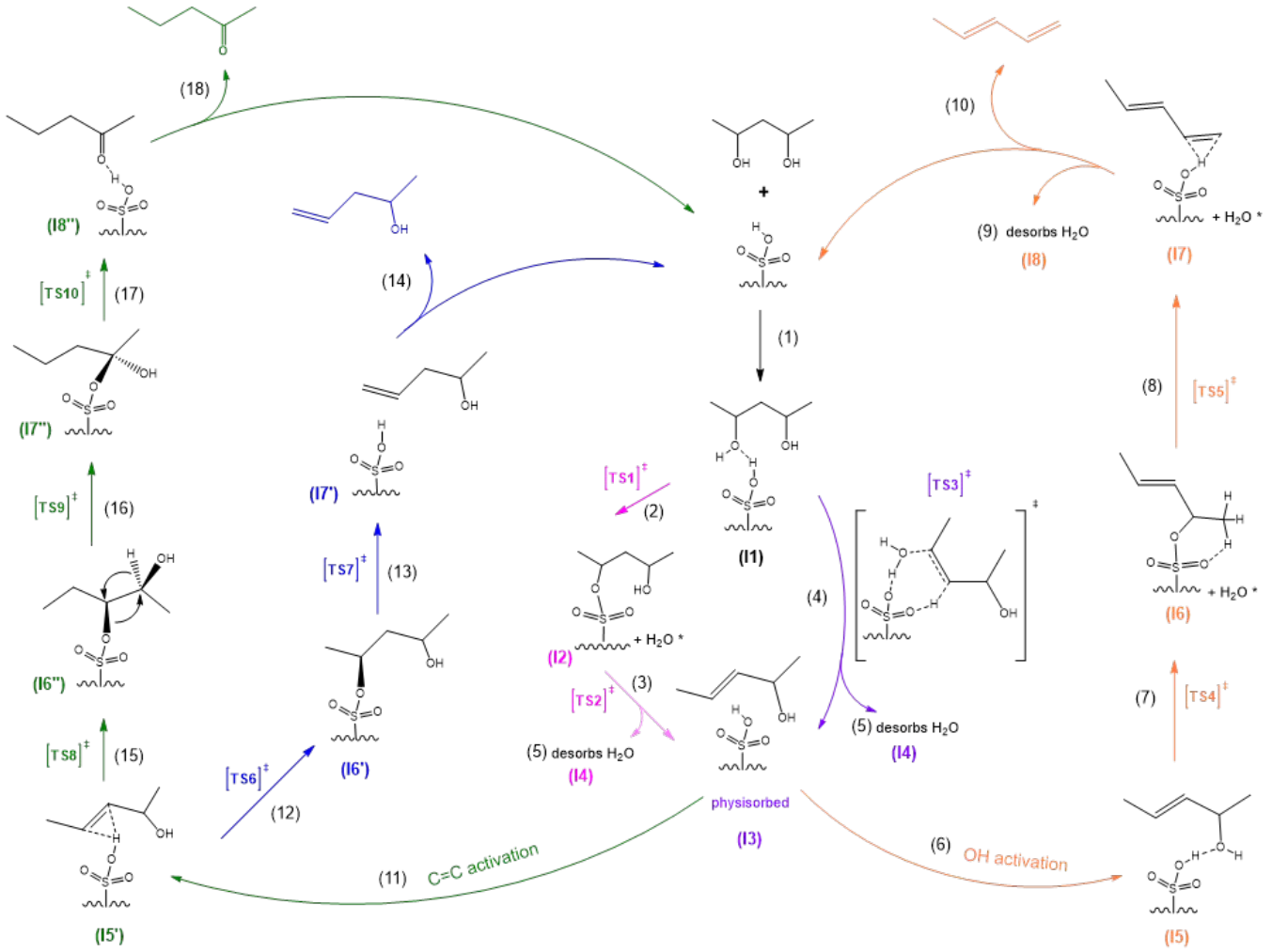

Figure 2. Proposed reaction mechanism. The elementary step is numbered in parentheses. The intermediate states are denoted by Ix, which also applies for Figures 3 and 4.

isomerization or the C=O group formation. The C=C bond isomerization is initiated with the formation of an alkoxide (I6') through the transition state TS6. The deprotonation of the intermediate I6' at the terminal CH_3 group results in an unsaturated alcohol that is a configurational isomer of the primary product. In the route of ketone formation, the C=O functional group could be firstly derived from the formation of a surface alkoxide (I6''). This intermediate is formed from the surface species I5' through the TS8 in an E1-like mechanism. The alkoxide I6'' then undergoes structural rearrangement through the TS9, in which the H atom at the carbon of OH group would be shifted to the carbon of the alkoxide group. This process leads to the formation of a hemi-ketal species (I7'') on the surface that contains both alkoxide and hydroxyl group at the same carbon atom. This intermediate proceeds through the TS10 to form a saturated ketone physisorbed on the surface (I8''). The ketone product then desorbs into the gas phase. In the following we discuss the energy profile of each elementary step.

3.1. Dehydration of the first hydroxyl group

Dehydration of the first OH group could occur via two plausible routes as depicted in Figure 3, which results in the formation of an unsaturated alcohol with internal C=C bonding (pent-3-en-2-ol) as the primary product. The change of Gibbs free energy upon adsorption of 2,4-pentanediol over the sulfonic group is -20 kJ/mol at 500 K, to which the enthalpic contribution is -50 kJ/mol (Table S1). Such a modest enthalpy change upon the adsorption suggests that the diol should be loosely bound to the surface, which implies the translation of adsorbate is restricted mostly in the direction perpendicular to the surface, while significant degrees of freedom in the rotational modes could remain. It is worth noting that alcohols physisorbed on BAS have been reported to proceed through a protonated form, stabilized by the negative charge remaining at the surface of the catalyst[40, 42]. However, such a protonated structure was not observed here. This difference could be attributed to the presence of a neighboring OH group, which withdraws electrons along the carbon chain and destabilizes the protonated hydroxyl group.

The stepwise dehydration of the first OH group starts with the formation of an alkoxide intermediate (I2) following an E1-like mechanism as shown in Figure 3. This step shows a positive change of Gibbs free energy, in which, physisorption of a water molecule over the adjacent sulfonic group (Figure S2) and the formation of surface alkoxide I2 reduces the entropic

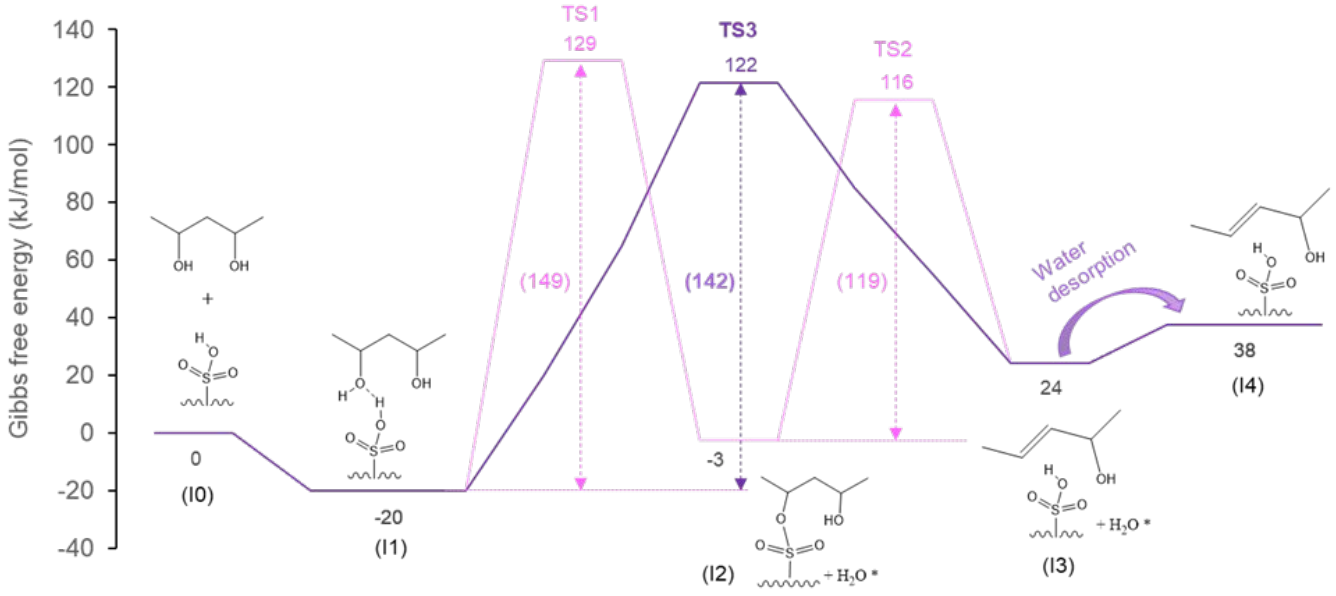

Figure 3. Gibbs free energy profile along reaction coordinates of the first -OH dehydration of diols. The numbers in parentheses are intrinsic activation barriers at the corresponding transition states. The intermediate is named with the text in parentheses, consistent with Figure 2.

compensation from the increased number of molecules. The Gibbs free energy of the intrinsic activation barrier is 149 kJ/mol, with a carbenium-like transition state (TS1). This observation is generally in line with the characteristic of a reaction following the E1 mechanism with an unstable carbenium transition state. However, in this study, the stability of TS1 should be further suppressed due to the electron-withdrawing effect of the neighboring OH group, which should exacerbate the energetic elevation of TS1.

To obtain further insight into the TS1, we analyzed the atomic structure. At the image of TS1, the dihedral angle among C1-C2-H2-C3 atoms is 172º, which strongly shows the planarity of a carbenium-characteristic structure (Figure S2). The oxygen (O2) atom of water is already 3.1 Å from the C2 atom while this carbon is still 2.9 Å from the oxygen (Os) of sulfonic group, which are, respectively, twice the C2-O2 bond length in the diol and the C2-Os bond length in the alkoxide intermediate (Figure S2). In addition, the C2-C3 bond length in the TS1 is still significantly shorter than that in both structures of the diol and the surface alkoxide (Figure S2). These characteristics reveal a middle transition state along the reaction coordinate, before combining with the sulfonate site to form the alkoxide intermediate. The entropy change upon the formation of TS1 is almost 50% more than that of the reaction (Table S2), which further indicates TS1 in a loose pair with the negative surface.

Deprotonation of the alkoxide I2 at the C3 atom (Figure S2) forms an unsaturated alcohol. The process is significantly endothermic due to the formation of a less thermodynamically stable product; however, the transformation of an alkoxide into the loosely physisorbed product on the surface leads to a high entropy gain. The intrinsic activation barrier is 119 kJ/mol, which is mostly attributed to the enthalpy change upon the formation of TS2 (Table S2).

Further analysis in the geometry of TS2 shows that this elementary step follows an E1-like mechanism. Figure S2 shows a large distance between C2 and Os and a closely planar geometry among C1-C2-H2-C3 atoms of the TS2 structure, which indicates that the C2-Os bond should be broken readily before the proton abstraction at the C3 atom takes place. However, the dihedral angle among C2-C3-H3'-C4 atoms of the TS2 (Figure S2) is 139º, far off the co-planar tri-angular hybridization of C-sp2 at C2-C3 atoms of the product. These observations suggest that the TS2 could be a middle transition state, but closer to the product. In fact, Figure 3 shows a comparable potential of the TS2 along the reaction coordinate with that of the TS1, which implies that the TS2 should have characteristics of a carbenium-like structure during the C3-H3 dissociation. It is also important to mention that similarly to the previous elementary step, the transition state TS2 in this deprotonation process could be further destabilized due to the electron-withdrawing effect of the neighboring OH group. Overall, the stepwise mechanism is rate-determined by the formation of the alkoxide intermediate (TS1).

In the concerted mechanism, elimination of the activated OH group and the proton abstraction at the C3 atom take place at the same reaction coordinate. The calculated Gibbs free energy of the intrinsic activation barrier is 142 kJ/mol, slightly lower than that of the stepwise mechanism hindered at the step of alkoxide formation. The result is consistent with the dehydration of alcohols over solid acids following the unimolecular route in the gas phase, in which the concerted mechanism was observed to be more kinetically favored than the stepwise E1-like mechanism involving the formation of surface alkoxide intermediate[41, 43].

The TS3 is a large cyclic transition state that involves simultaneously the C2-O1 bond cleavage and the C3-H3 deprotonation (Figure S2), which increases the rigidity of TS3 and thus reduces the entropy of system. This rigidity explains that the entropy compensation upon the formation of TS3 contributes insignificantly (~5%) to the Gibbs free energy

change of activation (Table S2). The distances in pairs of C2-O2 and C3-H3 are, respectively, 2.3 and 1.3 Å, which are large enough to be considered completed bond cleavage. The dihedral angle of 163º among C1-C2-H2-C3 atoms shows a sequential steps including C=C bond migration, intramolecular H4-shift, and hemi-ketalization).

3.2.1. Dehydration of the second hydroxyl group to form diene.

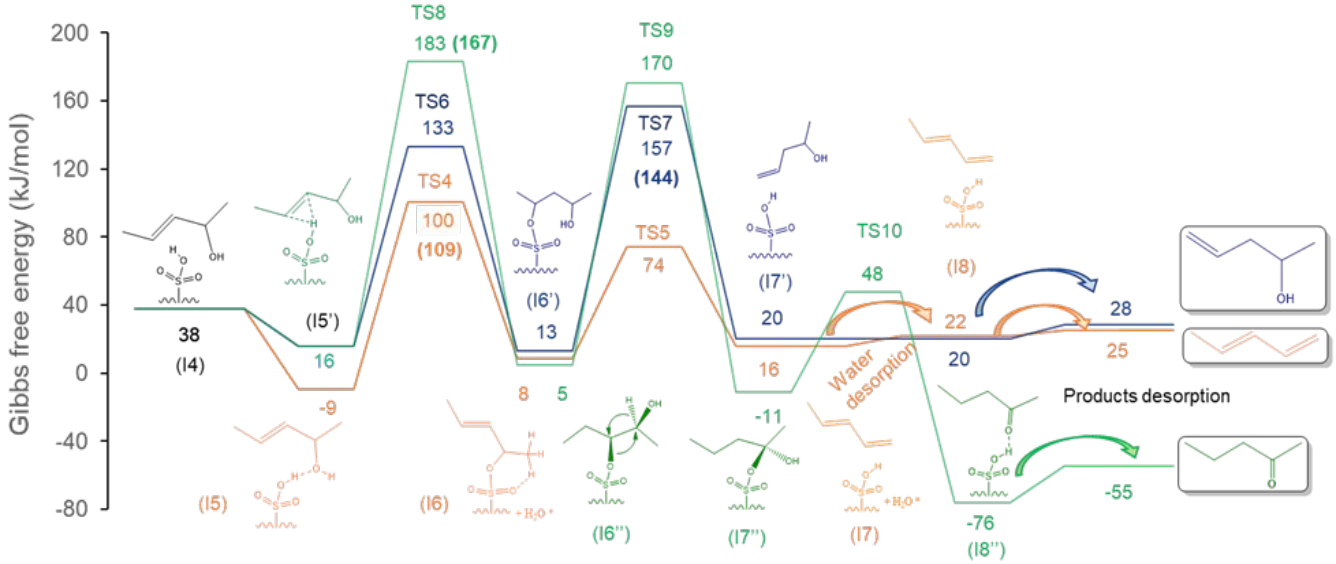

Figure 4. Gibbs free energy profile along the reaction coordinate of secondary conversions of the diol. The number in parentheses is the highest intrinsic activation barrier in the corresponding pathway. All energetic states are referenced to the gas-phase diol. Transition states and intermediates are indexed in parentheses the same as in Figure 2.

closed planar geometry to the configuration of a C-sp^2 at the C2 atom. However, the geometry at the C3 atom is observed with the dihedral angle of 133º among C2-C3-H3'-C4 atom, far off the planar characteristic of a C-sp^2, suggesting that the TS3 is a middle transition state that retains the characteristic of a carbenium[44].

The unsaturated alcohol (pent-3-ene-2-ol) generated in either the stepwise or the concerted mechanism stays at the sulfonic group; the C3 position in the molecule is 2.3 Å from the proton of the BAS. Activation of this physisorbed pent-3-ene-2-ol will be discussed in the next section. Overall, Figure 3 shows that the dehydration of the first OH group in the diol proceeds through the concerted mechanism, with a lower overall activation barrier compared to that of the stepwise mechanism (Figure 3, Table S2). The presence of a neighboring OH group is postulated to deplete the electron density at the carbenium site of TS1, decreasing its instability and hindering the formation of surface alkoxide intermediate.

3.2. Secondary conversions of the unsaturated alcohol

Figure 4 shows the Gibbs free energy profile of three plausible secondary conversions of the unsaturated alcohol that is the primary product in dehydration of the first OH group of the diol. We assume that this surface intermediate can change its conformation, due to its weak interaction with the surface, to be activated on the same sulfonic group. Its sequential reaction leads to the formation of a conjugated diene (via further dehydration of the second -OH group), an isomer of the primary product (via C=C bond migration), or a saturated ketone (via

Further dehydration of the unsaturated alcohol is initiated by activation of the remaining OH group. As shown in Figure S3, the carbon chain of pent-3-ene-2-ol slightly translates on top of the same acid site and axially rotates the C3-C4 bond so that the O4 atom of the hydroxyl group is towards the proton. This process of changing conformation is thermodynamically favorable with a Gibbs free energy change of -47 kJ/mol. The favorable adsorption could explain the experimental observation discussed below that only trace amounts of pent-3-ene-2-ol are detected during the conversion of diols, as the unsaturated alcohol can transform to secondary products.

This second dehydration process follows a unimolecular route with an E_1-like mechanism. Otherwise, the reaction coordinate for a concerted mechanism is limited due to lack of a basic site to abstract the H5 atom simultaneously with elimination of the activated OH group (Figure S3). As shown in Figure 4, the Gibbs free energy of activation for the formation of an alkoxide intermediate (I4) is 109 kJ/ mol. In the transition state TS4 (Figure S3), the distance between C4 and O4 atoms is 1.8 Å, which implies that the C-O bond is cleaved. However, a dihedral angle of 141º among C3-C4-H5'-C5 atoms indicates that the C4 atom is still reorganizing a C-sp3 structure into C-sp2. These characteristics show that the TS4 should be rather an early transition state, with a carbenium-like structure towards the formation of alkoxide I4 (Figure S3). The occurrent C=C bond at the C2-C3 position with the electronic-donating conjugated effect lowers the potential surface along the reaction coordinate of alkoxide formation, leading to the

significantly lower activation barrier in the calculations than that of the equivalent step in the first dehydration.

In the deprotonation step, a Gibbs free energy of the intrinsic activation barrier to abstract the H5 atom from surface alkoxide I4 is 66 kJ/mol (Figure 4). The process is more facile than the equivalent step in the first dehydration. In the transition state TS5 (Figure S3), the distance between C5 and H5 atoms is 1.3 Å, which implies that the C-H bond is cleaved. The co-planar geometry among C3-C4-H5'-C5 atoms with a dihedral angle of 172º indicates that π-bonding between C4 and C5 atoms is nearly established. In addition, the length of bonds inside the TS5 is very close to that of the dienes product (Figure S3). These characteristics show that the TS5 is a late transition state with a carbenium-like structure. The conjugated C=C bonds distribute more uniformly the positive charge within the TS5 via the electronic-donating effect and thus further stabilize the transition state. As a result, the activation barrier in this case is significantly reduced in comparison with that of the equivalent step in the first dehydration.

The diene product stays on top of the active site, at which the newly generated C=C bond shows a moderately exothermic interaction with the BAS (Table S1). Figure 4 shows an almost neutral Gibbs free energy of desorption, which suggests that the diene product could easily desorb into the gas phase; this may be different from the EVOH co-polymer as the latter's product desorption is less favored due to the stronger interaction (see discussion later). The theoretical apparent activation barrier for conversion from the diol into the diene product was computed using the energetic span model[36], and the result is discussed in section 3.2.4.

3.2.2. Migration of the C=C bond in the unsaturated alcohol. Different from the aforementioned secondary dehydration, the C=C bond in the primary product (an unsaturated alcohol) can also migrate along the carbon chain catalyzed by the acid site. Accordingly, the pent-3-ene-2-ol first slightly translates so that the C=C bond is on top of the proton (Figure S4) with a Gibbs free energy change of -22 kJ/mol. Next, formation of two different alkoxides at either C2 or C3 atoms can take place (Figure 2, Figure S4), leading to an isomer of the primary unsaturated alcohol or a saturated ketone.

The migration of the C=C bond is induced by the formation of a surface alkoxide (I6') at C2 (Figure S4), which takes place via an electrophilic addition mechanism. In the transition state TS6, the proton is pairing with the C3 atom that leads to the formation of a carbenium-like structure at the C2 position. This elementary step could be considered an inverse deprotonation step of the first dehydration following the E_1-like mechanism that is previously discussed in section 3.1.2, as the surface alkoxide I6' is in fact the identical structure with the surface alkoxide I2 (Figure 2). Indeed, Figure 4 shows that the Gibbs free energy of intrinsic activation barrier of this step, if referenced to the physisorbed primary product, is 95 kJ/mol, which is essentially identical to that of the backward activation barrier of the deprotonation step in the first dehydration. Furthermore, Figure S4 shows that the TS6 has similar geometries with the TS2. These observations suggest that, despite the first dehydration being kinetically facile via the concerted mechanism, the formation of alkoxides I2 or I6' could still be possible.

In the next step, the surface alkoxide I6' undergoes the proton abstraction at the terminal methyl group, resulting in pent-4-ene-1-ol, an isomer of the primary product with the migrated C=C bond on the carbon chain. The Gibbs free energy of the intrinsic activation barrier is 144 kJ/mol, which is dominated by a high enthalpic change of 156 kJ/mol to cross the transition state TS7 (Table S2). Figure S4 shows that despite being closer to the product, the TS7 rather retains the carbenium-like characteristics of a middle transition state. This result explains the higher intrinsic activation barrier for this step compared to the equivalent step in the first dehydration, which could be attributed to a lower stability of the TS7, a carbenium-like transition state with less substituted alkyl group than the TS2. The similar trend in structural stability of the carbenium transition state has also been observed by Kostestkyy et al.[45] and Kang et al.[46] during dehydration of various alcohols over solid acids. Overall, Figure 4 shows that the rate-determining step in this secondary conversion involves the deprotonation process to recover the BAS**.**

3.2.3. Formation of the ketone functional group. A surface alkoxide at the C3 atom (Figure S5) can also form through the transition state TS8. The Gibbs free energy of the intrinsic activation barrier of this step is 167 kJ/mol, which is attributed to a very high enthalpic change upon the formation of the TS8. Figure S5 shows that the proton of the sulfonic group is already bonded with the C2 atom in the TS8. In addition, the dihedral angle of 174º among C2-C3-H3'-C4 atoms shows the planar geometry of coordination of C3 atom, indicating a middle transition state of TS8 in the form of a carbenium-like structure. The result implies that the stability of TS8 could be significantly suppressed due to the electron-withdrawing effect of the neighboring OH group. Accordingly, this explains the fact that, despite both surface alkoxides at C2 and C3 showing comparable thermodynamic stability on the energetic profile (Figure 4) and being derived from the same activated precursor (Figure 2), the intrinsic activation barrier of this elementary step is much higher than that of the equivalent step in the C=C bond migration.

In the next step, the surface alkoxide I6'' proceeds via an intramolecular shift of H4 from the C4 to the C3 position to form a hemi-ketal intermediate I7'' (Figure 2). In fact, this type of 1,2-structural rearrangement has been observed in organic chemistry, in which the mechanism involves an intramolecular transfer of the hydride from the carbon with the OH group to the next carbon atom on the chain[47, 48]. A similar mechanism was also suggested by Thomas et al.[15] for the formation of

ketone groups during the thermal degradation of PVA. Here we found an analogous mechanism that is plausible for this conversion over a heterogeneous catalyst, which has been inadequately addressed in the literature. The Gibbs free energy of the intrinsic activation barrier of this elementary step is 165 kJ/mol, determined by a pronounced enthalpic cost to reach the transition state TS9 (Table S2). As shown in Figure S5, the basic oxygen of the sulfonic group is equidistant (2.5 Å) to either C3 or C4 atoms of the TS9. In addition, the length of the C3-C4 bond (1.4 Å) is very close to that of a typical carbenium-like structure, and the transferred hydrogen is close to the center of C3-C4 bond. These characteristics imply that the positive charge in TS9 should be distributed in the vicinity of the C3-H4-C4 triangle. Therefore, we suggest that the transfer process could be possibly a proton shift along with the reversible formation of π-bonding between C3 and C4 atoms, rather than a hydride transfer. Further analysis in the dihedral angles among the coordination of C3 and C4 centers in the TS9 shows that the transformation of C4 into a C-sp2 is still in progress, while such a process should be completed at C3 (Figures S5). This result implies that a larger portion of the positive charge in the TS9 should be unevenly localized at the C3 atom. Accordingly, this transition state could be considered a carbenium-like structure coordinating with the proton being transferred from C4 to C3, in which the charge center is closer to C3.

In the final step, the surface hemi-ketal I7'' proceeds with the deprotonation of the OH group to form the ketone (C=O) functional group at C4 atom. The Gibbs free energy of the intrinsic activation barrier is 59 kJ/mol, which is mostly attributed to a mild enthalpic change of 61 kJ/mol to approach the transition state TS10. Figure S5 shows that the distance between C4 and Os is 1.9 Å, which indicates the scission of this C-O bond has been just completed. In addition, the dihedral angle among C3-C4-O4-C5 atoms in the TS10 is 143º that is still far off that in the ketone product, which suggests that TS10 should be an early transition state that is much closer to the surface hemi-ketal I7''. Indeed, latter images along the reaction coordinate of this step depict that the TS10 quicky transforms into an oxocarbenium structure before deprotonating the OH group to form the C=O bond. The observation suggests that the density of positive charge on the C4 atom during the formation of TS10 should be alleviated by the resonance from lone pairs of electrons on the O4 oxygen. As a result, the stability of TS10 could be further increased, which reduces significantly the activation barrier of this step compared to the other corresponding to carbenium-like structures observed in this study. A similar phenomenon was also reported by Chia et al.[49] during the conversion of polyols in biomass upgrading.

Figure 4 shows that the ketone product is substantially distinct in the thermodynamic stability, which extends the energetic barrier between the highest transition state (TS8) and the lowest intermediate (I7'') in two consecutive catalytic cycles of the secondary conversion compared to the other two reaction pathways. Accordingly, the formation of a surface alkoxide next to the OH group is the rate-determining step of this ketone formation pathway.

3.2.4. Comparison of different reaction pathways. To figure out the rate-determining intermediate (RDI) among the surface species and the rate-determining transition state (RDTS), we applied the energetic span model as described in the literature[36]. In fact, the calculated Gibbs free energy including underestimated entropies of the surface species computed by the harmonic approximation as in this study could lead to exponential errors in the absolute energetic states. It is also noticed that another factor that should be further considered is the surface coverage of intermediate species[50], which requires microkinetic analysis. In this study, however, we utilized this model to qualitatively assess the RDI and RDTS in each separate reaction pathway and to compare the trend in the calculated apparent activation barrier of reaction pathways with the experimental selectivity of secondary products.

Figure S6 depicts two consecutive catalytic cycles of the diene formation pathway. Table S3 shows that the RDI is the OH activated form of the primary product in the first cycle, while the TS3 during the first OH dehydration via the concerted mechanism is the RDTS. The result suggests that the conversion of such a diol into the conjugated dienes product should be mostly hindered by the stability of the transition state during the first dehydration, whereas the process could be rationally promoted with a longer residence time and/or a stronger interaction of the unsaturated alcohol intermediate (the primary product) with the active site over the surface. The theoretical apparent activation barrier of this diene formation route is 156 kJ/mol, the lowest among the three parallel, secondary pathways. Accordingly, the conjugated diene should be dominant with respect to other secondary products, which is consistent with the experimental data shown in Figure 5.

A similar analysis was performed for the route of C=C bond migration. The RDI and the RDTS are, respectively, the adsorbed diol at the beginning and the TS7 in the secondary conversion of the same cycle (Figure S7 and Table S3). This characteristic implies that such C=C bond migration process should be limited by the stability of the transition state during the H-b abstraction of surface alkoxide intermediates. The Gibbs free energy of the apparent activation barrier is 177 kJ/mol, which is significantly higher than that of the diene formation. As a result, the product selectivity resulting from C=C bond migration should be lower than the dienes product, which is consistent with experimental observations shown in Figure 5. Nevertheless, it should be noted that a high activation barrier upon the formation of TS7 should be reduced when the equivalent step takes place on a second-degree carbon (-CH_2-) instead of the terminal CH_3 group as in this study. Accordingly, we anticipate that this C=C bond migration process should be more competitive than the further dehydration in case of the same reaction occurring on the EVOH co-polymer, which possibly lowers the efficiency of deoxygenation via the elimination of OH groups.

In the ketone formation pathway, the TS8 is determined as the RDTS while the RDI is the adsorbed state of either diol reactant or the ketone product (Figure S8 and Table S3). One possible RDI is the adsorbed ketone product (I8''), which accounts for 55% degrees of rate control weighted on surface intermediates. The computed apparent activation barrier of ketone formation pathway with the RDI of I8" is 204 kJ/mol of Gibbs free energy, which is yet much higher than those of the C=C bond migration and further dehydration. This result is attributed to the fact that the substantial thermodynamic stability of ketone product, corresponding to the very unstable carbenium-like transition state TS8, highly elevates the activation barrier and thus hinders this process compared to other pathways. Another possible RDI of this reaction pathway is the adsorbed diol at the beginning of catalytic cycle, which results in 203 kJ/mol of Gibbs free energy of the apparent activation barrier. This could rather be interpreted that the selectivity of ketone should only be hindered due to the instability of TS8, rather than the distinct thermodynamic stability of the ketone product. In both cases, significant Gibbs free energies of the apparent activation barriers are observed, which is consistent with the lowest selectivity of the ketone product compared to the others (see experimental results and discussion). These results show that despite the great thermodynamic favorability, the conversion of such a diol into ketone should be kinetically restricted mostly at the formation of a surface alkoxide intermediate that proceeds through a carbenium transition state at C-β relatively to the OH group.

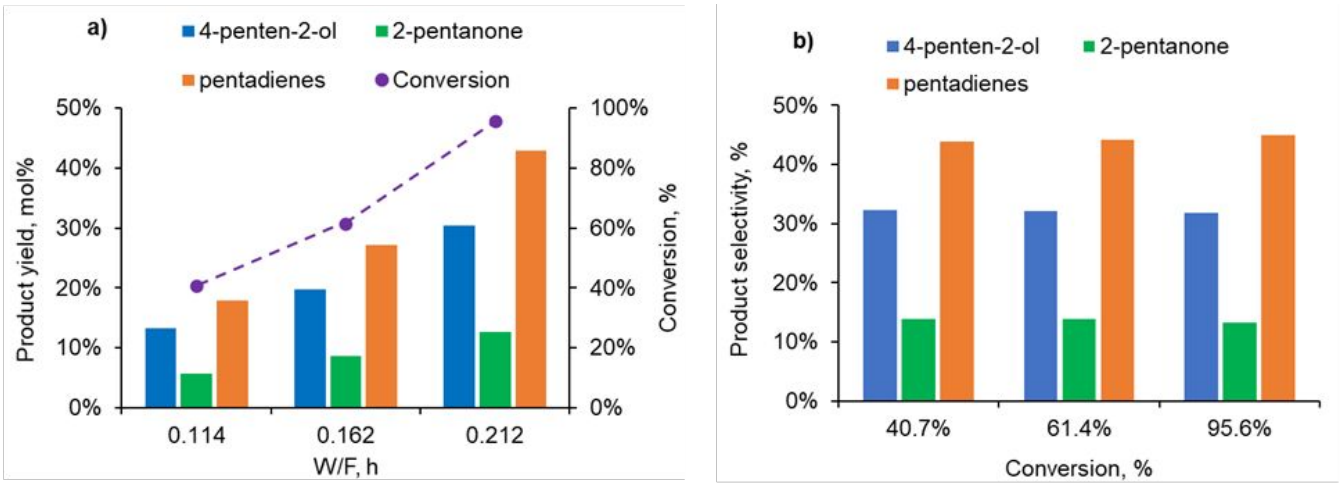

Figure 5. Experimentally measured conversion and product yield. a) Initial conversion and product yields; **b)** Product selectivity of 2,4-pentanediol conversion over sulfonic-functionalized amorphous silica. Reaction conditions: T = 200 °C, $P_{2,4\text{-pentanediol}}$ = 0.3 kPa.

3.3. Experimental results of pentanediol dehydration

It has been reported that the dehydration of pentanediol over solid catalyst could form various products such as alkenol, diene, ketone, and aldehyde.[18, 19] In this study, different products in the vapor phase dehydration of 2,4-pentanediol are detected based on GC-FID and GC-MS results, including pentadiene isomers, 4-pentene-2-ol, 2-pentanone, an insignificant amount of pentene, and only trace amounts of 3-pentene-2-ol. The conversion, product yield, and product selectivity resulting from the reaction of 2,4-pentanediol with respect to varying reaction space time, which is defined as the catalyst mass/reactant flowrate (W/F), are shown in Figure 5.

A trace amount of 3-pentene-2-ol was detected, indicating that this alkenol compound is more likely to be the active primary product. The high thermodynamic favorability of such a "direct" activation of the unsaturated alcohol intermediate as shown in the DFT calculations should play a more pronounced role in the build-up of this gaseous primary product than the desorption and re-adsorption back to the surface from the gas phase.

As shown in Figure 5a, the conversion of 2,4-pentanediol increases linearly with W/F, indicating that it is not influenced by thermodynamic equilibrium under the reaction conditions. It is noticed that all the product yields keep increasing with the increase of the 2,4-pentanediol conversion. In addition, the selectivity of pentadiene isomers (secondary dehydration product), 4-pentene-2-ol (C=C bond migration product), and 2-pentanone (ketone pathway product) remain unchanged with increasing conversion (Figure 5b). This observation may imply that either sequential reactions may occur along the diffusion path of the crystal, limiting equilibration with gas-phase species,[51] or that the rate of desorption of the first dehydrated product is comparable to the rates of sequential reactions of surface species. However, given the energy and product desorption barriers (Figure 4), it is more likely that the three major observed products are formed in parallel, and 4-penten-2-ol is probably not the primary product of the first dehydration step. Additionally, the product yields over a wide range conversion in Figure 5a show that pentadiene is the most abundant product, followed by 4-pentene-2-ol and 2-pentanone, respectively. This observation could be attributed to the different energy barriers of secondary conversions, which is in line with the trend of DFT-calculated activation barriers for forming these products.

It should be noted that there was a small product yield of the other unidentified products, which could be the oligomers of pentadiene, varying from 0.6 to 1.5% with increasing the reaction space time from 0.114 to 0.212 h. In the calculations, as we focused on the acid-catalysed unimolecular reactions, oligomerization nor polymerization was thus not included

3.4. Relevance to conversion of EVOH

The results and discussion above on the conversion of 2,4-pentanediol, as a model compound of EVOH, provides valuable insights for the selective conversion of this co-polymer. In particular, the mechanism of activation of the primary product via slightly changing of adsorption conformation suggests that the selectivity of products could be less affected by the diffusion process from/to the surface of the partially dehydrated EVOH. Instead, the formation of surface alkoxides should play a more pronounced role in the kinetics. Accordingly, it is anticipated that in the early stage of the reaction when the content of hydroxyl groups is high, the dehydration to form conjugated C=C bonds could be dominant regardless of the surface coverage of alkoxide. However, when the ratio of C=C bond in the structure is increased, the surface coverage of such intermediates could be more kinetically relevant for the migration of C=C bond and the ketone formation, suppressing the further dehydration reaction.

In addition, when the C=C bond migration takes place in the EVOH, its kinetics should be mostly altered by the internal -CH_2- groups, rather than the terminal CH_3- group in the diol. The methylene group provides a higher stability for the carbenium-like transition state. As a result, a reduced intrinsic activation barrier of the deprotonation step could possibly vary the selectivity of C=C migration with respect to the further dehydrated product.

Furthermore, as the formation of ketones is kinetically restricted at the formation of surface alkoxides at C-β of the unsaturated alcohol, tailoring the local environment can increase the stability of the transition state for this elementary step and consequently enhance the conversion of EVOH into the C=O functionalized product. Utilizing confinement and/or sufficient hydrophilicity of the solvent system is thus postulated to facilitate the proton transfer in surface intermediates, which promotes ketone formation in selective conversion of EVOH as shown in our previous work[52].

4. Conclusions

Based on theoretical calculations and experiments on the model compound, we show that the partial dehydration of PVA co-building blocks in EVOH can generate conjugated dienes, isomers of unsaturated alcohol, and ketone. The experimental observation agrees with the DFT-calculated reaction profiles. Moreover, through intramolecular proton shift, the unsaturated alcohol can be converted to ketone over the heterogeneous Brønsted acid sites; this proton transfer can in principle be facilitated by protic solvents and thus introduce new functionality (the ketone groups) into the polymer. This intramolecular proton transfer is also very relevant to hydrodeoxygenation in biomass upgrading, in which C5-polyalcohols are abundant in the feedstock. These insights can be integrated into the recycling of plastics and biomass conversion with additional functional groups (C=C and C=O double bonds). This new functionality allows further polymer conversion to produce valuable chemicals.

Author Contributions

Quy P. Nguyen: Methodology, Investigation, Formal analysis, Visualization, Writing – original draft.

Han K. Chau: Methodology, Investigation, Formal analysis, Visualization, Writing – original draft.

Lance Lobban: Writing – review & editing.

Steven Crossley: Writing – review & editing.

Bin Wang: Conceptualization, Writing – review & editing.

Conflicts of interest

There are no conflicts to declare.

Acknowledgements

The work has been supported by the National Science Foundation under grant no. EFRI E3P-2029394. We thank Dai-phat Bui for the SEM imaging. The computational work was performed at the OU Supercomputing Centre for Education & Research and the National Energy Research Scientific Computing Centre (NERSC), a U.S. Department of Energy Office of Science User Facility.

Notes and references

1. T. I. Butler and B. A. Morris, in *Multilayer flexible packaging*, Elsevier, 2016, pp. 281-310.
2. T. Anukiruthika, P. Sethupathy, A. Wilson, K. Kashampur, J. A. Moses and C. Anandharamakrishnan, *Comprehensive Reviews in Food Science and Food Safety*, 2020, **19**, 1156-1186.
3. U. Kanbur, G. Zang, A. L. Paterson, P. Chatterjee, R. A. Hackler, M. Delferro, I. I. Slowing, F. A. Perras, P. Sun and A. D. Sadow, *Chem*, 2021, **7**, 1347-1362.
4. X. Jia, C. Qin, T. Friedberger, Z. Guan and Z. Huang, *Science advances*, 2016, **2**, e1501591.
5. V. Dufaud and J. M. Basset, *Angewandte Chemie International Edition*, 1998, **37**, 806-810.
6. C. T. de Mello Soares, M. Ek, E. Östmark, M. Gällstedt and S. Karlsson, *Resources, Conservation and Recycling*, 2022, **176**, 105905.
7. M. Niaounakis, *Recycling of flexible plastic packaging*, William Andrew, 2019.
8. K. Kaiser, M. Schmid and M. Schlummer, *Recycling*, 2017, **3**, 1.

9. K. L. Sánchez-Rivera, P. Zhou, M. S. Kim, L. D. González Chávez, S. Grey, K. Nelson, S. C. Wang, I. Hermans, V. M. Zavala and R. C. Van Lehn, *ChemSusChem*, 2021, **14**, 4317-4329.
10. T. W. Walker, N. Frelka, Z. Shen, A. K. Chew, J. Banick, S. Grey, M. S. Kim, J. A. Dumesic, R. C. Van Lehn and G. W. Huber, *Science advances*, 2020, **6**, eaba7599.
11. P. Zhou, K. L. Sánchez-Rivera, G. W. Huber and R. C. Van Lehn, *ChemSusChem*, 2021, **14**, 4307-4316.
12. M. C. Mulakkal, A. C. Castillo, A. C. Taylor, B. R. Blackman, D. S. Balint, S. Pimenta and M. N. Charalambides, *Resources, Conservation and Recycling*, 2021, **166**, 105371.
13. I. Kremer, T. Tomić, Z. Katančić, M. Erceg, S. Papuga, J. Parlov Vuković and D. R. Schneider, *Clean Technologies and Environmental Policy*, 2022, **24**, 677-693.
14. B. Morris, *The Science and Technology of Flexible Packaging. Oxford: William Andrew Publishing*, 2017, 69-119.
15. P. Thomas, J.-P. Guerbois, G. Russell and B. Briscoe, *Journal of thermal analysis and calorimetry*, 2001, **64**, 501-508.
16. H. Yang, S. Xu, L. Jiang and Y. Dan, *Journal of Macromolecular Science, Part B*, 2012, **51**, 464-480.
17. D. Sun, Y. Yamada, S. Sato, S. Suganuma and N. Katada, *Applied Catalysis A: General*, 2016, **526**, 164-171.
18. F. Sato, H. Okazaki and S. Sato, *Applied Catalysis A: General*, 2012, **419**, 41-48.
19. M. K. Gnanamani, G. Jacobs, W. D. Shafer, S. D. Hopps and B. H. Davis, *ChemistrySelect*, 2017, **2**, 4150-4156.
20. T. Kondo, T. Sasaki, S. Ruiz-Barragan, J. Ribas-Ariño and M. Shiga, *Journal of Computational Chemistry*, 2021, **42**, 156-165.
21. G. Kresse and J. Furthmüller, *Physical review B*, 1996, **54**, 11169.
22. P. E. Blöchl, *Physical review B*, 1994, **50**, 17953.
23. G. Kresse and D. Joubert, *Physical review b*, 1999, **59**, 1758.
24. J. P. Perdew, K. Burke and M. Ernzerhof, *Physical review letters*, 1996, **77**, 3865.
25. S. Grimme, J. Antony, S. Ehrlich and H. Krieg, *The Journal of chemical physics*, 2010, **132**, 154104.
26. G. Henkelman and H. Jónsson, *The Journal of chemical physics*, 2000, **113**, 9978-9985.
27. G. Henkelman and H. Jónsson, *The Journal of chemical physics*, 1999, **111**, 7010-7022.
28. A. Heyden, A. T. Bell and F. J. Keil, *The Journal of chemical physics*, 2005, **123**, 224101.
29. B. A. De Moor, A. Ghysels, M.-F. Reyniers, V. Van Speybroeck, M. Waroquier and G. B. Marin, *Journal of Chemical Theory and Computation*, 2011, **7**, 1090-1101.
30. C. J. Cramer, *Journal*, 2004.
31. C. T. Campbell and J. R. Sellers, *Journal of the American Chemical Society*, 2012, **134**, 18109-18115.
32. G. Piccini and J. Sauer, *Journal of chemical theory and computation*, 2014, **10**, 2479-2487.
33. M. Jørgensen and H. Gronbeck, *The Journal of Physical Chemistry C*, 2017, **121**, 7199-7207.
34. L. H. Sprowl, C. T. Campbell and L. Arnadottir, *The Journal of Physical Chemistry C*, 2016, **120**, 9719-9731.
35. B. A. De Moor, M.-F. Reyniers and G. B. Marin, *Physical Chemistry Chemical Physics*, 2009, **11**, 2939-2958.
36. S. Kozuch and S. Shaik, *Accounts of Chemical Research*, 2011, **44**, 101-110.
37. A. Comas-Vives, *Physical Chemistry Chemical Physics*, 2016, **18**, 7475-7482.
38. G. Li, B. Wang, B. Chen and D. E. Resasco, *Journal of Catalysis*, 2019, **377**, 245-254.
39. H. Chiang and A. Bhan, *Journal of Catalysis*, 2010, **271**, 251-261.
40. D. Mei and J. A. Lercher, *The Journal of Physical Chemistry C*, 2019, **123**, 25255-25266.
41. M. John, K. Alexopoulos, M.-F. Reyniers and G. B. Marin, *Journal of Catalysis*, 2015, **330**, 28-45.
42. C. M. Nguyen, M.-F. Reyniers and G. B. Marin, *Journal of Catalysis*, 2015, **322**, 91-103.
43. M. A. Christiansen, G. Mpourmpakis and D. G. Vlachos, *Acs Catalysis*, 2013, **3**, 1965-1975.
44. S. Roy, G. Mpourmpakis, D.-Y. Hong, D. G. Vlachos, A. Bhan and R. Gorte, *Acs Catalysis*, 2012, **2**, 1846-1853.
45. P. Kostestkyy, J. Yu, R. J. Gorte and G. Mpourmpakis, *Catalysis Science & Technology*, 2014, **4**, 3861-3869.
46. M. Kang, J. F. DeWilde and A. Bhan, *ACS catalysis*, 2015, **5**, 602-612.
47. R. C. van der Drift, E. Bouwman and E. Drent, *Journal of organometallic chemistry*, 2002, **650**, 1-24.
48. T. Xia, Z. Wei, B. Spiegelberg, H. Jiao, S. Hinze and J. G. de Vries, *Chemistry–A European Journal*, 2018, **24**, 4043-4049.
49. M. Chia, Y. J. Pagán-Torres, D. Hibbitts, Q. Tan, H. N. Pham, A. K. Datye, M. Neurock, R. J. Davis and J. A. Dumesic, *Journal of the American Chemical Society*, 2011, **133**, 12675-12689.
50. Z. Mao and C. T. Campbell, *ACS Catalysis*, 2019, **9**, 9465-9473.
51. S. P. Crossley, D. E. Resasco and G. L. Haller, *Journal of Catalysis*, 2019, **372**, 382-387.
52. H. K. Chau, Q. P. Nguyen, A. C. Jerdy, D.-P. Bui, L. L. Lobban, B. Wang and S. P. Crossley, *ACS Catalysis*, 2023, **13**, 1503-1512.